Encapsulation of methylammonium lead bromide perovskite in nanoporous GaN ᴱᴾ

Kevin T. P. Lim ⁱᴰ, Callum Deakin ⁱᴰ, Boning Ding, Xinyu Bai, Peter Griffin ⁱᴰ, Tongtong Zhu ⁱᴰ, Rachel A. Oliver ⁱᴰ, and Dan Credgington ⁱᴰ

COLLECTIONS

Paper published as part of the special topic on Perovskite Semiconductors for Next Generation Optoelectronic Applications

ᴱᴾ   This paper was selected as an Editor's Pick

View Online   Export Citation   CrossMark

ARTICLES YOU MAY BE INTERESTED IN

Dielectric and ferroic properties of metal halide perovskites
APL Materials 7, 010901 (2019); https://doi.org/10.1063/1.5079633

Suppression of non-radiative recombination toward high efficiency perovskite light-emitting diodes
APL Materials 7, 021102 (2019); https://doi.org/10.1063/1.5064370

Enhanced photovoltaic performance of perovskite solar cells by Co-doped spinel nickel cobaltite hole transporting layer
APL Materials 7, 021101 (2019); https://doi.org/10.1063/1.5079954

Encapsulation of methylammonium lead bromide perovskite in nanoporous GaN (EP)

View Online   Export Citation   CrossMark

Kevin T. P. Lim,[1,a)] (iD) Callum Deakin,[2,a)] (iD) Boning Ding,[2] Xinyu Bai,[1] Peter Griffin,[2] (iD) Tongtong Zhu,[2] (iD)
Rachel A. Oliver,[2] (iD) and Dan Credgington[1,b)] (iD)

AFFILIATIONS

[1] Cavendish Laboratory, University of Cambridge, JJ Thomson Avenue, Cambridge CB3 0HE, United Kingdom

[2] Department of Materials Science and Metallurgy, University of Cambridge, 27 Charles Babbage Road,
 Cambridge CB3 0FS, United Kingdom

Note: This paper is part of the special topic on Perovskite Semiconductors for Next Generation Optoelectronic Applications.
[a)]**Contributions:** K. T. P. Lim and C. Deakin contributed equally to this work.
[b)]**Author to whom correspondence should be addressed:** djnc3@cam.ac.uk

ABSTRACT

Halide perovskites hold exceptional promise as cheap, low temperature solution-processed optoelectronic materials. Yet they are hindered by poor structural and chemical stability, rapidly degrading when exposed to moisture or air. We demonstrate a solution-phase method for infiltrating methylammonium lead bromide perovskite ($CH_3NH_3PbBr_3$, or $MAPbBr_3$) into nanoporous GaN which preserved the green photoluminescence of the perovskite after up to 1 year of storage under ambient conditions. Besides a protective effect, confinement within the porous GaN matrix also resulted in a blueshift of the perovskite emission with decreasing pore size, suggesting an additional templating effect of the pores on the size of the perovskite crystals within. We anticipate that our method may be generalised to related perovskite materials, offering a route to producing composites of interest for use in optoelectronic devices for various applications.

Halide perovskites (ABX$_3$, where A is a monovalent metal or organic cation, B is a Group 14 metal or metalloid such as Ge, Sn, or Pb, and X is a halide such as Cl, Br, or I) have emerged as promising next-generation luminescent materials due to their spectral tunability, narrow emission, high quantum efficiency, as well as affordability and solution processability. These desirable qualities may enable the creation of cheap and versatile perovskite light sources with a wide colour reproduction range, excellent colour purity, high brightness, and low power usage. However, in many halide perovskites, the exciton binding energy is low enough that excitons can spontaneously dissociate into free electrons and holes at room temperature.[1] This reduces radiative recombination rates, allowing non-radiative trap-assisted recombination at defect sites to compete and lower the achievable quantum efficiency at low carrier density.[2–4] Halide perovskites also tend to be unstable to ambient air and moisture,[5] and this instability may be

exacerbated by migration of ionic species in a device under electrical bias.[6]

Encapsulation within an impermeable matrix of a more stable material is one strategy for protecting perovskites from environmental degradation. Perovskites encapsulated in nanoporous titania,[7] alumina,[8,9] silica,[10] and silicon[9] have been demonstrated to remain stable on timescales ranging from 1 day to 1.5 months (see Table S1 of the supplementary material). In addition to providing protection, nanoporous matrices also act as physical templates that force perovskites to adopt a nanoparticulate form. This confinement can enhance the probability of radiative recombination and thus the luminescent efficiency by increasing the overlap of electron and hole wavefunctions in the perovskite: electrons and holes in the perovskite experience a stronger attraction when the surrounding medium has a low dielectric constant which provides poor electrostatic screening

("dielectric confinement"), and electrons and holes are confined into a small volume by internal reflection of their wavefunctions at potential steps at the boundaries of the perovskite nanocrystal ("spatial confinement"). When the scale of spatial confinement is smaller than the exciton Bohr radius[9] in the perovskite, strong quantum confinement of the carriers increases their energy, resulting in blueshifted emission.

Gallium nitride (GaN) is an inorganic semiconductor used in optoelectronic devices due to its direct band gap in the UV, optical transparency, electrical and thermal conductivity, chemical stability, as well as high decomposition temperature. Recent reports have demonstrated methods for the porosification of epitaxial GaN by selective electrochemical etching of highly doped GaN layers.[11,12] This opens up the possibility of large-scale infiltration of perovskites into porous GaN as a low-temperature post-processing step, creating a composite material. Such a composite would be particularly amenable to optoelectronic device integration. For instance, a prefabricated epitaxial GaN light-emitting diode (LED) could subsequently be combined with an infiltrated perovskite phosphor for tuning the emission wavelength. The GaN alloy family is the standard for UV and blue LED technology, but is less effective for longer wavelength devices without downconversion. Current narrow-emission phosphors have limitations, particularly in terms of their response time. By contrast, perovskite phosphors have the potential for excellent colour rendering and high modulation bandwidths, sufficient for applications in solid-state lighting and visible light communication.[13]

Here, we present a method for infiltrating methylammonium lead bromide perovskite (MAPbBr$_3$, MA = CH$_3$NH$_3^+$) into nanoporous GaN and characterise the resulting perovskite/GaN composite material. MAPbBr$_3$ was chosen as a suitable model perovskite due to its bright emission in the visible spectrum and large absorption coefficient[14] in the UV and blue on the order of 10^5 cm^{-1}. Based on this value, a few microns of perovskite/GaN composite phosphor with a 10% filling fraction of perovskite would absorb >99% of UV or blue excitation to first approximation. The GaN/MAPbBr$_3$ system has also been reported to form a Type I heterojunction[15] with the band gap of GaN straddling that of MAPbBr$_3$, which could enhance carrier confinement by suppressing carrier wavefunction leakage from the perovskite.

To form the nanoporous template, GaN epitaxial layers on sapphire were electrochemically etched with 0.25 M aqueous oxalic acid as electrolyte, following a protocol previously reported in Ref. 12. Under application of a constant potential difference between the GaN sample and a Pt counter electrode, n-doped layers of GaN were selectively porosified due to their high conductivity. Non-intentionally doped (NID) layers are not conductive, and so there is no electric field at the NID GaN/electrolyte interface and these parts of the material are not etched. In a typical sample, a thin top layer of GaN was n-doped with Si to a concentration of 1×10^{19} cm^{-3} and thus porosified, while a thicker NID base layer (Si concentration <10^{17} cm^{-3}) remained intact. The etching voltage was varied to produce a variety of pore sizes and shapes. We analysed the

surface porosity by measuring scanning electron micrographs (SEMs) of the etched surfaces (Fig. 1).

Etching GaN at a potential of 6 V relative to Pt afforded a pitted surface [Fig. 1(a)] with many shallow round pores (diameter 11–14 nm) as well as fewer elongated pores (long dimension 17–26 nm) likely formed by the merging of two round pores. The etching extends vertically to create short channels [Fig. 1(d)]. A higher potential of 8 V resulted in a denser coverage of pores [Fig. 1(b)], comprising round pores (diameter 14–17 nm) and asymmetric pores of various shapes and sizes merged from several round pores (up to 40–80 nm long). A diagonal cross section created by a sloping cleaved edge reveals a sponge-like porous structure [Fig. 1(e)]. Finally, a 10 V etch created an open and connected pore morphology [Fig. 1(c)] with a few round pores (diameter 16–20 nm) and majority of the pore volume in an irregular porous network with deeper voids and channels and a highly variable length scale of porosity (100–200 nm at the longest). The openness of the pore network is particularly evident in the cross-sectional view in Fig. 1(f). This trend in the GaN porosity is consistent with the observation in Ref. 16 that pore morphology changes with etching voltage. Etching voltages below 6 V did not result in any noticeable porosification, while a voltage of 12 V resulted in extensive porosification that compromised the integrity of the porous layer. As such, we limited our investigation to the use of GaN etched at 6 V, 8 V, and 10 V.

Multiple possible routes exist to achieve perovskite infiltration into porous substrates. While co-evaporation as a deposition method has been shown to yield perovskites of high quality on planar substrates, it is incompatible with infiltration into a solid porous matrix as it is a directional, line-of-sight technique and can only fill directly exposed pores on the surface. Instead, most work on encapsulation of perovskites in a matrix of another material has used solution-processing methods on porous layers that are very thin (<100 nm)[9] or open (typically spin-cast from a solution of nanoparticles),[17,18] or even avoids the problem of infiltration entirely by depositing the matrix on the perovskites.[8]

These reports often use the one-step deposition technique, in which the perovskite crystallises from a precursor solution directly onto a substrate or into a template. In the case of spin-coating of nanoparticles, the template is formed simultaneously with the crystallisation of the perovskite. Due to the strong driving force for perovskite crystallisation from solution, the reaction proceeds rapidly and can result in uneven filling of the porous template or the creation of pre-formed crystallites in solution.[19] For our porous GaN system, we established that this tended to result in poorer pore filling, likely due to clogged pores near the surface hindering deeper infiltration of material into the template.

We found the use of the alternative two-step deposition method to achieve a greater extent of pore infiltration. This method involves initial deposition of the lead halide precursor, preferably in a "wet" amorphous state that remains permeable to solvent molecules and ions, followed by a slow solid-state reaction with the organic precursor to convert it into
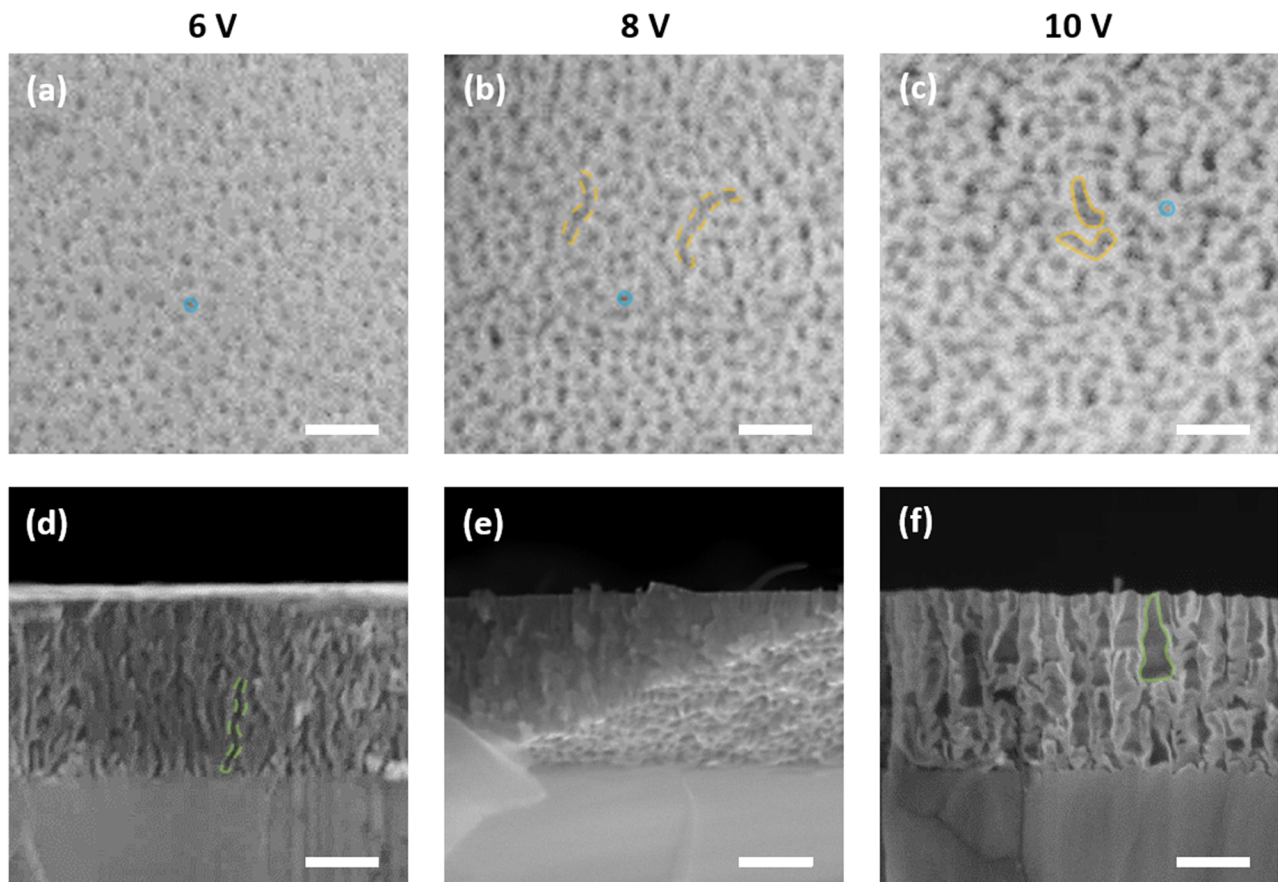
FIG. 1. SEM micrographs of porous GaN obtained by etching at 6 V [(a) and (d)], 8 V [(b) and (e)], and 10 V [(c) and (f)]. [(a)–(c)] Top surface of porous GaN imaged at a tilt angle of 45°, in which pores can be seen as dark spots and patches on a bright background. With increased etching voltage, small round pores (blue outlines) grow and merge (orange dashed outlines) to give longer, more asymmetric pores (orange outlines). [(d)–(f)] Cleaved edges of the etched samples imaged in cross-section, showing a sharp transition between the porous GaN layer and the underlying un-etched NID GaN. The vertical direction corresponds to the *c*-axis of wurtzite GaN. At low etching voltages (d), the pores extend vertically into isolated channels (green dashed outline). At higher etching voltages (f), some lateral etching is evident, such that the channels to form a porous network with large open pockets (green outline). The vertical channels are hidden in (e) which cleaved at a sloping angle, giving rise to a honeycomb appearance instead. Scale bars: 100 nm [(a)–(c)] and 200 nm [(d)–(f)].

perovskite. This process is illustrated schematically in Fig. 2 and proceeds as follows.

A 1.0 M solution of $PbBr_2 \cdot 2DMSO$ in dimethylformamide (DMF) and a 0.1 M solution of MABr in isopropanol (IPA) were prepared. Substrates were cleaned by ultrasonication in acetone and IPA, and subsequently subjected to a 15–20 min oxygen plasma treatment at a power of 50 W to render the surface hydrophilic for optimal wetting of the solutions. For a 1 cm square substrate, 30 μl of the $PbBr_2 \cdot 2DMSO$ solution was dropped onto the substrate and left undisturbed for
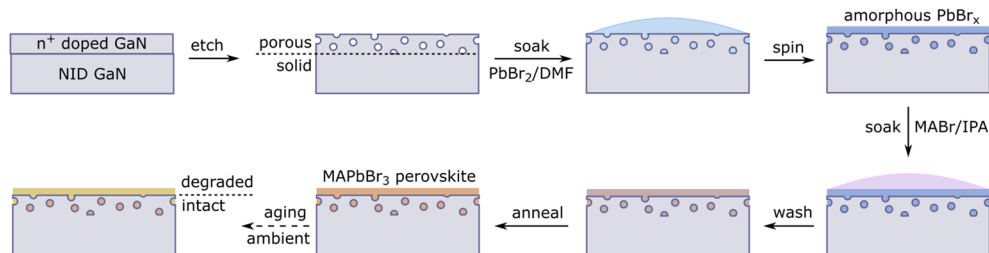
FIG. 2. Process flow for a low-temperature solution process for obtaining perovskite/GaN composites.

at least 1 min to soak into the porous surface. Thereafter, the substrate was spun at 2000 rpm for 20 s to evaporate DMF from the droplet and form the $PbBr_2 \cdot 2DMSO$ precursor film, which we also refer to as (amorphous) $PbBr_2$ film for convenience.

Next, 60 μl of the MABr solution was dropped onto the substrate and left undisturbed for 10–20 min in a closed Petri dish for MABr to incorporate into the $PbBr_2$ film. The excess MABr was removed by two washes with 1 ml pure IPA. Finally, the substrates were annealed on a hotplate at 80 °C for 15–20 min to crystallise the perovskite. (Annealing at higher temperatures was found to be detrimental to the formation of the perovskite.)

This method is well-suited for pore infiltration as it is easier for the amorphous $PbBr_2$ formed in the first step to achieve uniform surface coverage and pore filling as compared to direct deposition of $MAPbBr_3$ perovskite, which tends to crystallise rapidly into discrete nanocrystals instead of forming a continuous film.

To establish the structure of the sample, we used a focussed ion beam (FIB) microscope to prepare a cross-sectional TEM lamella for tandem scanning transmission electron microscopy and energy dispersive X-ray spectroscopy (STEM-EDX) studies.

A cross-sectional high-angle annular dark-field (HAADF) STEM image of the sample is shown in Fig. 3(a). The bulk and porous GaN layers are clearly resolved, whilst a capping layer of perovskite and platinum protective coating is also visible. EDX elemental maps acquired from the region of the lamella defined by the orange box in Fig. 3(a) are shown in Figs. 3(b)–3(d) for gallium (Ga), lead (Pb), and bromine (Br), respectively. Regions of Fig. 3(b) that show a weak Ga signal are seen to match dark regions in the HAADF-STEM image, i.e., the positions of the pores. From a visual comparison of the EDX maps, these porous regions of low Ga content also appear to be enriched in Pb and Br as compared to the surrounding material in Figs. 3(c) and 3(d), which suggests some degree of pore infiltration.

To support these claims, we analysed the spatial correlations between the Ga, Pb, and Br elemental maps, as plotted in Figs. 3(e) and 3(f). In Fig. 3(e), the negative correlation between the Pb and Ga signals is consistent with Pb being located within the pores of GaN. First, the porosity of GaN imposes an upper bound (dashed line) on the maximum volume that can be filled with Pb, with the Pb counts suppressed to the baseline level in regions with high Ga counts (low porosity). We note that the baseline of the Pb signal is non-zero as the measured Pb peak overlaps with a strong Ga peak which is present throughout the mapped area (see Fig. S1 of the supplementary material). Second, the vertical spread of points below the dashed line at lower Ga counts reflects a range of possible Pb concentrations at any porosity, with the upper bound of Pb volume fraction seldom reached. Taken together, these observations are indicative of the presence of Pb in the GaN pores, but with an incomplete and variable extent of filling. We attribute this incomplete pore filling to voids created in the film by shrinkage of the $PbBr_2 \cdot 2DMSO$ precursor in its conversion to $MAPbBr_3$ perovskite.
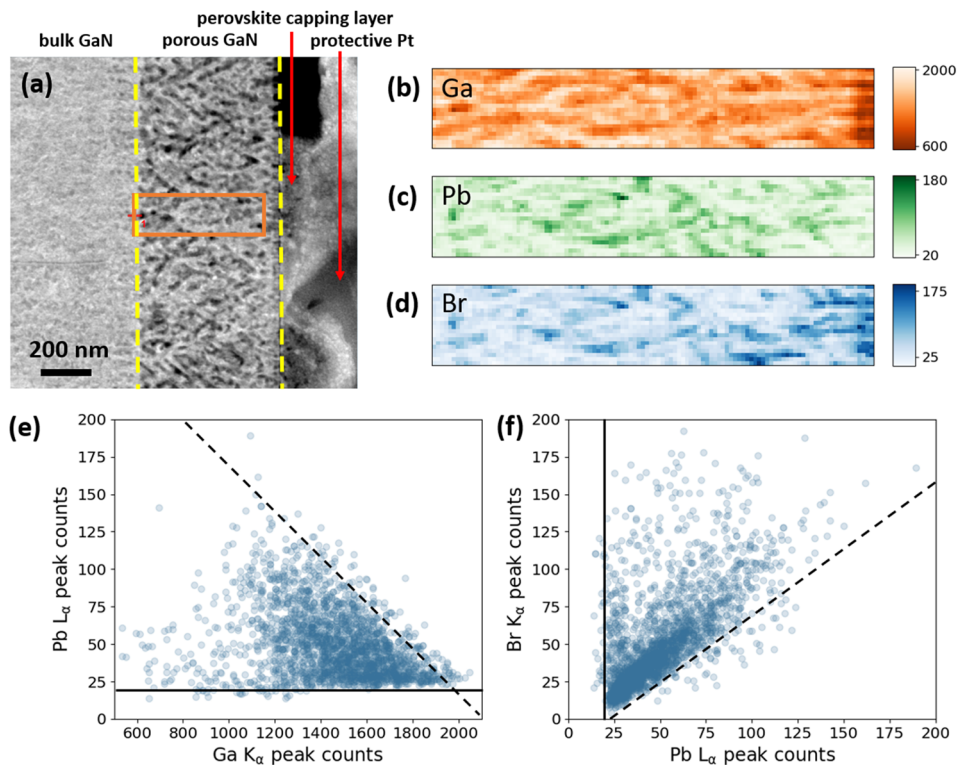
FIG. 3. Cross-sectional STEM-EDX characterisation of a perovskite/GaN composite, in which EDX elemental mapping was performed on the highlighted region (orange box) of the perovskite-infiltrated porous GaN layer in the HAADF-STEM image (a). EDX elemental maps of the boxed area (20 × 110 pixels), showing the number of counts at the chosen peak for each element: (b) gallium (Ga-K_α), (c) lead (Pb-L_α), and (d) bromine (Br-K_α). Plots of the spatial correlation between the signal intensity measured for the elements in [(b)–(d)]: (e) Pb vs Ga, and (f) Br vs Pb. Overlapping data points appear as darker areas in the plot. Lines are a guide to the eye (solid lines: Pb baseline; dashed lines: positive and negative correlation trends). Representative spectra from these data sets can be found in the supplementary material (Fig. S1).

In Fig. 3(f), the positive correlation between the Br and Pb signals is consistent with these elements occurring together in compounds such as $PbBr_2$ or $MAPbBr_3$. Most of the points lie above the dashed line, which implies a lower bound on the ratio of Br to Pb as would be expected from a reaction in which MABr incorporates into $PbBr_2$. However, we are unable to determine if the limiting stoichiometry that defines the lower bound is that of $PbBr_2$, $MAPbBr_3$, or some other related phase. Above the dashed line, the slope of Br against Pb takes on a range of values corresponding to various stoichiometries of MA_xPbBr_{2+x}, suggesting varying degrees of MABr incorporation. The vertical spread of points at the lowest Pb counts (Br/Pb ratio tending to infinity) may be due to small inclusions of MABr that infiltrated the pores but did not incorporate into $PbBr_2$. As the lack of suitable standards and correction factors precludes conversion of the measured EDX count ratios to relative atomic concentrations by Cliff-Lorimer analysis, it is difficult to determine with certainty if any substantial fraction of $MAPbBr_3$ is present based on elemental analysis alone.

Having established the presence of Pb and Br within the porous GaN, we next investigated the nature of the material containing these elements using photoluminescence (PL) spectroscopy. PL spectra of the composite material show a characteristic green emission, confirming the formation of $MAPbBr_3$ perovskite in the pores of GaN. PL measurements also allow us to investigate two effects arising from the interaction between the perovskite and its porous scaffold: encapsulation and confinement. We observe both a protective effect due to a slowing of environmental degradation and a templating effect as seen in a pore size-dependent shift of the PL peak wavelength due to nanoscale confinement.

To investigate the protective effect of the porous GaN substrates on the encapsulated perovskite, we deposited perovskites on glass, non-porous GaN, and porous GaN (GaN with a porous top layer 200 nm in thickness). Each substrate was cleaved to give two equivalent samples, with one left open to air and the other sealed, using epoxy to mount it face-down onto a glass coverslip. Samples were then left to age for 10 days in ambient atmosphere. As seen in the PL spectra in Fig. 4, the PL intensity of all samples under equivalent excitation conditions decreased with aging. The sealed samples maintained an appreciable level of PL intensity after 10 days, whereas almost no PL signal could be detected from perovskite deposited on unsealed glass and non-porous GaN substrates. By contrast,

perovskite infiltrated into porous GaN retained 25% of the initial PL intensity even without sealing, suggesting a protective effect of the porous GaN matrix on the perovskite in its pores.

While measuring PL intensities is relatively straightforward, accurately measuring optical absorption is difficult due to scattering in the bulk of our thick perovskite/GaN-on-sapphire samples, and particularly from the unpolished back of the sapphire substrate. To determine whether the relative change in PL intensity over time reflects an underlying drop in sample quantum yield, the absolute external PL quantum efficiency (PLQE) of the perovskite on selected GaN samples was measured using an integrating sphere. For unsealed porous GaN, the PLQE dropped from 1.65% to 0.93% after 10 days of aging in ambient atmosphere, qualitatively similar to the relative decrease evident in Fig. 4(c). After 350 days (50 weeks) in ambient conditions, unsealed glass and non-porous GaN samples exhibited faint emission barely visible by eye with PLQE <0.10%, whereas the porous GaN samples were still brightly emissive with a PLQE of 0.60% (36% of the initial PLQE as made). To our knowledge, this yearlong survival of unsealed perovskite in ambient conditions is one of the longest durations reported at the time of writing, which may support the use of GaN as an encapsulant for perovskites. A comparison of previous reports on perovskite stability in nanoporous matrices of other materials is given in the supplementary material (see Table S1).

In order to account for the portion of PL intensity that is lost during ambient aging, we consider that some fraction of the total luminescence initially arises from the capping layer of perovskite on the surface of the porous GaN, as depicted schematically in Fig. 2. As the capping layer is unprotected, it is reasonable that this contribution to the PL should degrade in the same manner as the planar layers deposited on glass and non-porous GaN, leaving only the PL contribution from perovskite in the pores of porous GaN.

To investigate the templating effect of the pores on perovskite formation, we deposited perovskites on GaN substrates of differing porosities obtained by performing the electrochemical etching step at voltages of 6 V, 8 V, and 10 V. Increasing the etching voltage over this range increased the minimum observed diameter of an individual pore from approximately 11 nm to 16 nm, while also causing pores to merge into trenches and channels with longer and irregular shapes (Fig. 1). For these samples, the concentrated $PbBr_2$
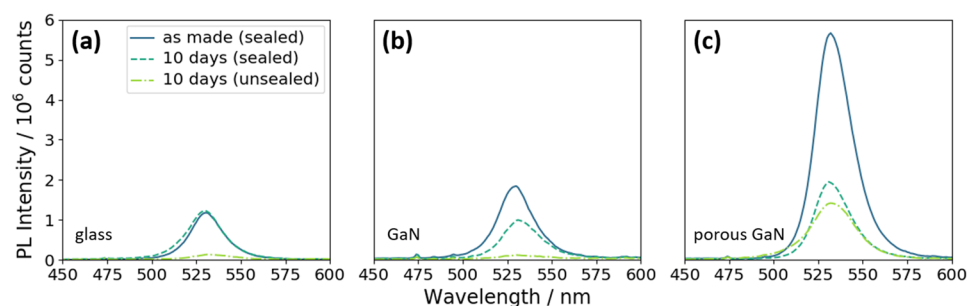
FIG. 4. Protective effect of porous GaN on perovskites: PL spectra for $MAPbBr_3$ perovskite deposited on (a) glass, (b) non-porous (un-etched) GaN, and (c) GaN incorporating a 200 nm porous layer etched at 10 V, indicating the decrease in PL intensity after 10 days in ambient atmosphere with and without epoxy-glass sealing.
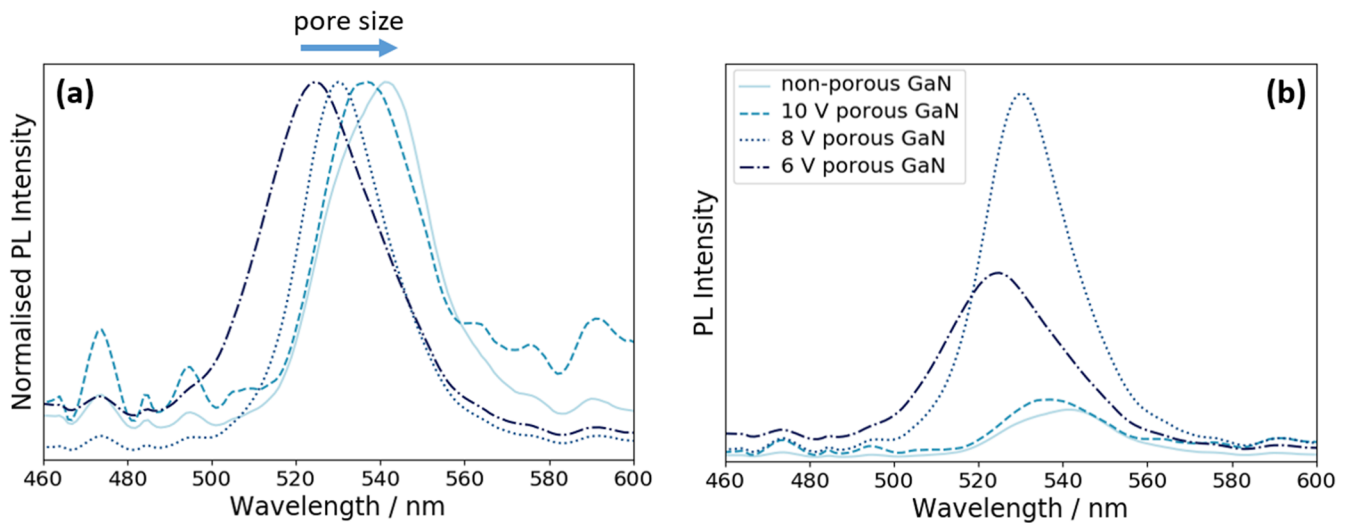
FIG. 5. Templating effect of porous GaN on perovskites: comparison of PL spectra of perovskites deposited on GaN substrates porosified to a depth of 1000 nm with different etching conditions (non-porous GaN, and porous GaN etched at 6 V, 8 V, and 10 V). (a) Blueshift in PL peak wavelength with decreasing pore volume. Peak intensities are normalised for clarity. The blue arrow is a guide to the eye. (b) Variation in PL peak intensity with porosity. The 8 V porous GaN sample shows the strongest PL. Characteristics of the emission peaks are listed in Table I.

solution on the substrate was washed off after the soaking step and replaced with a dilute PbBr$_2$ solution to reduce the thickness of the capping layer formed during spin-coating. This was done before the MABr solution soaking and annealing steps and was required to decrease the fraction of luminescence arising from the capping layer, which could otherwise mask any confinement-induced blueshift of the PL peak wavelength associated with luminescence from perovskites in the pores. To boost the strength of the luminescence signal from pore-confined perovskite, the thickness of the porous layer was also increased to 1000 nm so as to increase the amount of perovskites in the pores. As a control, a non-porous (unetched) substrate was directly spin-coated with dilute PbBr$_2$ solution.

We observed a systematic blueshift of the PL peak wavelength from 541 nm to 525 nm going from non-porous GaN to 6 V-etched porous GaN [Fig. 5(a)], which is suggestive of increasing confinement due to the perovskite being forced to occupy pores of decreasing size. We note, however, that the luminescence wavelength can be very sensitive to variations in preparation conditions. In particular, the MABr soaking step and annealing step control the extent to which MABr is incorporated into the PbBr$_2$ film and thus the final material composition MA$_x$PbBr$_{2+x}$, which affects the luminescence wavelength. The blueshift trend is only observed when the perovskite preparation process is carefully controlled.

We also observed a strong enhancement of the PL intensity with 8 V porous GaN and a smaller but still significant increase for 6 V porous GaN as compared to non-porous and 10 V porous GaN [Fig. 5(b)]. This hints at the existence of an optimal porosity for perovskite/GaN composites, which could be due to the difficulty of infiltrating and retaining the

perovskite in pores of either too small or too large a volume. If so, the low PL intensity for perovskites deposited on 10 V porous GaN may simply be due to the limited amount of material retained in the large open pore network after washing. On the other hand, the pores and the porous area in 6 V porous GaN are relatively small, and so may not accommodate as much perovskite as 8 V porous GaN. The main features of the PL spectra in Fig. 5 are summarised in Table I.

For a more quantitative analysis of the confinement effect, we calculated the average expected sizes of the crystallites responsible for the blueshifted PL by fitting the peak wavelengths to the Brus equation[20]

$$E^* = E_g + \frac{\hbar^2 \pi^2}{2\mu R^2} - \frac{1.8 e^2}{4\pi \varepsilon_0 \varepsilon_r R}, \tag{1}$$

where $E^* = hc/\lambda$ is the energy of the photons emitted at the PL peak wavelength λ, and R is the radius of the crystallites to be determined.

Using values from Ref. 21 of bulk band gap E_g = 2.292 eV, exciton reduced mass μ = 0.117 m_0 (in units of electron mass), and effective dielectric constant ε_r = 7.5, we obtain

TABLE I. PL characteristics of GaN samples etched with decreasing etching voltage (decreasing pore size). Non-porous GaN is unetched. Data taken from Fig. 5.

	Peak wavelength (nm)	Relative peak intensity	FWHM (nm)
Non-porous	541	1.00	27
10 V porous	537	1.19	30
8 V porous	530	7.13	24
6 V porous	525	3.65	34

crystallite diameters of 14 nm, 11 nm, and 10 nm for the 10 V, 8 V, and 6 V samples, respectively. These values compare favourably with the pore sizes of the different etched GaN substrates that we measured from SEM images, albeit being consistently 10%–20% smaller than the smallest pore sizes. This result is physically reasonable and is likely to reflect incomplete pore filling due to shrinkage of the precursor film upon transformation into perovskite. Finally, since the perovskite remains luminescent within the GaN pores and a blueshift in emission is observed, neither electron-hole separation (which might be expected to quench emission) nor the formation of interface states (which might be expected to redshift luminescence) is likely to be significant, consistent with Type I band alignment between the perovskite and GaN.

In summary, we have demonstrated a low-temperature solution process for creating perovskite/GaN composite materials by infiltrating two-step deposited $MAPbBr_3$ perovskite into nanoporous GaN. In the resulting composite, environmental degradation of the GaN-encapsulated perovskite is significantly slowed, with the green photoluminescence from the perovskite preserved even after prolonged storage of up to 1 year in ambient atmosphere. A porosity-dependent blueshift of the emission peak wavelength and the trend in the emission intensity were also observed. As our method involves only a simple sequence of soaking and spin-coating steps, we believe that it could also be adapted to work with similar halide perovskites such as $CsPbBr_3$. Such composites offer the potential for simple modification of efficient GaN LEDs to emit over a tunable range. With further development, we envision perovskite/GaN composites as a platform for facile and modular fabrication of optoelectronic devices, where the properties of the composite can be tuned by altering the conditions used for GaN growth, GaN etching, and perovskite processing.

See the supplementary material for details of perovskite preparation and storage (section A), the experimental detail of photoluminescence measurements (section B) and of STEM-EDX analysis (section C). Figure S1 shows example STEM-EDX spectra from two representative pixels of a pore and a region between pores. Table S1 presents a comparison of perovskite stability in other nanoporous media reported in literature.

REFERENCES

[1]A. Miyata, A. Mitioglu, P. Plochocka, O. Portugall, J. T. W. Wang, S. D. Stranks, H. J. Snaith, and R. J. Nicholas, Nat. Phys. **11**, 582 (2015).
[2]Y. H. Qiu, F. Nan, Q. Wang, X. D. Liu, S. J. Ding, Z. H. Hao, L. Zhou, and Q. Q. Wang, J. Phys. Chem. C **121**, 6916 (2017).
[3]Y.-H. Kim, H. Cho, and T.-W. Lee, Proc. Natl. Acad. Sci. U. S. A. **113**, 11694 (2016).
[4]G. Xing, B. Wu, X. Wu, M. Li, B. Du, Q. Wei, J. Guo, E. K. L. Yeow, T. C. Sum, and W. Huang, Nat. Commun. **8**, 14558 (2017).
[5]J. S. Manser, M. I. Saidaminov, J. A. Christians, O. M. Bakr, and P. V. Kamat, Acc. Chem. Res. **49**, 330 (2016).
[6]T. A. Berhe, W.-N. Su, C.-H. Chen, C.-J. Pan, J.-H. Cheng, H.-M. Chen, M.-C. Tsai, L.-Y. Chen, A. A. Dubale, and B.-J. Hwang, Energy Environ. Sci. **9**, 323 (2016).
[7]J. Burschka, N. Pellet, S.-J. Moon, R. Humphry-Baker, P. Gao, M. K. Nazeeruddin, and M. Grätzel, Nature **499**, 316 (2013).
[8]A. Loiudice, S. Saris, E. Oveisi, D. T. L. Alexander, and R. Buonsanti, Angew. Chem., Int. Ed. **56**, 10696 (2017).
[9]S. Demchyshyn, J. M. Roemer, H. Groiß, H. Heilbrunner, C. Ulbricht, D. Apaydin, A. Böhm, U. Rütt, F. Bertram, G. Hesser, M. C. Scharber, N. S. Sariciftci, S. Bauer, E. D. Głowacki, and M. Kaltenbrunner, Sci. Adv. **3**, e1700738 (2017).
[10]D. N. Dirin, L. Protesescu, D. Trummer, I. V. Kochetygov, S. Yakunin, F. Krumeich, N. P. Stadie, and M. V. Kovalenko, Nano Lett. **16**, 5866 (2016).
[11]C. Zhang, S. H. Park, D. Chen, D. W. Lin, W. Xiong, H. C. Kuo, C. F. Lin, H. Cao, and J. Han, ACS Photonics **2**, 980 (2015).
[12]T. Zhu, Y. Liu, T. Ding, W. Y. Fu, J. Jarman, C. X. Ren, R. V. Kumar, and R. A. Oliver, Sci. Rep. **7**, 45344 (2017).
[13]I. Dursun, C. Shen, M. R. Parida, J. Pan, S. P. Sarmah, D. Priante, N. Alyami, J. Liu, M. I. Saidaminov, M. S. Alias, A. L. Abdelhady, T. K. Ng, O. F. Mohammed, B. S. Ooi, and O. M. Bakr, ACS Photonics **3**, 1150 (2016).
[14]B. Wenger, P. K. Nayak, X. Wen, S. V. Kesava, N. K. Noel, and H. J. Snaith, Nat. Commun. **8**, 590 (2017).
[15]J. Gong, S. Liu, Y. He, X. Feng, X. Xia, Z. Quan, and L. Wang, Appl. Phys. Lett. **111**, 122103 (2017).
[16]G. Wang, S. Fu, L. Chen, J. Wang, X. Qin, Y. Wang, Z. Zheng, and Q. Duanmu, J. Semicond. **31**, 116002 (2010).
[17]A. Kojima, M. Ikegami, K. Teshima, and T. Miyasaka, Chem. Lett. **41**, 397 (2012).
[18]G. Li, Z. K. Tan, D. Di, M. L. Lai, L. Jiang, J. H. W. Lim, R. H. Friend, and N. C. Greenham, Nano Lett. **15**, 2640 (2015).
[19]K. Yan, M. Long, T. Zhang, Z. Wei, H. Chen, S. Yang, and J. Xu, J. Am. Chem. Soc. **137**, 4460 (2015).
[20]L. E. Brus, J. Chem. Phys. **80**, 4403 (1984).
[21]K. Galkowski, A. Mitioglu, A. Miyata, P. Plochocka, O. Portugall, G. E. Eperon, J. T. W. Wang, T. Stergiopoulos, S. D. Stranks, H. J. Snaith, and R. J. Nicholas, Energy Environ. Sci. **9**, 962 (2016).